Direct Visualizing the Spin Hall Effect of Light via Ultrahigh-Order Modes

Hailang Dai,[1] Luqi Yuan,[1,*] Cheng Yin,[3] Zhuangqi Cao,[1] and Xianfeng Chen[1,2,†]
[1]The State Key Laboratory on Fiber Optic Local Area Communication Networks and Advanced Optical Communication Systems, School of Physics and Astronomy, Shanghai Jiao Tong University, Shanghai 200240, China
[2]Collaborative Innovation Center of Light Manipulations and Applications, Shandong Normal University, Jinan 250358, China
[3]Jiangsu Key Laboratory of Power Transmission and Distribution Equipment Technology, Hohai University, Changzhou 213022, China

(Received 5 September 2019; accepted 16 January 2020; published 4 February 2020)

We report an experiment showing the submillimeter Imbert-Fedorov shift from the ultrastrong spin-orbital angular momentum coupling, which is a photonic version of the spin Hall effect, by measuring the reflection of light from the surface of a birefringent symmetrical metal cladding planar waveguide. The light incidents at a near-normal incident angle and excites resonant ultrahigh-order modes inside the waveguide. A 0.16-mm displacement of separated reflected light spots corresponding to two polarization states is distinguishable by human eyes. In our experiment, we demonstrate the control of polarizations of light and the direct observation of the spin Hall effect of light, which opens an important avenue towards potential applications for optical sensing and quantum information processing, where the spin nature of photons exhibits key features.

DOI: 10.1103/PhysRevLett.124.053902

The spin-orbit interaction of photons on the interface with the refractive-index inhomogeneity corresponds to the interplay between the spin degree of freedom of light and the extrinsic orbital angular momentum, which is a photonic version of the spin Hall effect [1–3]. It leads to a perpendicular spin-dependent displacement of light, i.e., the so-called Imbert-Fedorov (IF) shifts [4,5]. For many measurements of the spin Hall effect of light (SHEL), the displacement between two opposite spins is at the order of the wavelength of light, which cannot be distinguishable by human eyes. The quantum weak measurement technology [6–11] therefore has been utilized, which desires a complex experimental setup and hence limits potential practical applications [9,11]. On the other hand, the general concept of SHEL associated with the polarization nature of light occurs universally in many optical systems [10]. It leads to the longitudinal Goos-Hänchen shift from the spatial dispersion of light and also the transverse IF shift [7,9], which originates from the geometric Berry phase and the conservation of normal components of the total angular momentum of light [10]. Because of the unique physical nature [5–9] as well as possible implications in the metrology and the spin-based nano-optics [10,11], the research of SHEL is of important interest [12–14]. In particular, a large number of experimental works with the quantum weak measurement have been performed to observe the IF shift at a variety of optical platforms including the air-dielectric interface [15–20], metamaterial with the photon tunneling process [12], metasurfaces [17,21–24], Weyl semimetals [25], heterostructure semiconductors [26], and thin films supporting leaky guided modes [27], where the quantum noise of light limits the efficiency of the measurement [11]. Recently, methods associated with the surface plasmon resonance (SPR) have been applied to enhance the SHEL [27–30]. For example, an enhancement with a factor of 50 is revealed for the light incident on the metal surface near the Brewster angle, which gives the IF shift $\sim 3.2\ \mu$m [30]. Moreover, a small incident angle for the enhancement of SHEL in hyperbolic metamaterials has been explored and the transverse beam shift is $\sim 9\ \mu$m [31]. A natural question arises: is there a system supporting an IF shift associated with the SHEL that is large enough to be distinguished by human eyes?

In this Letter, we show an ultrastrong spin-orbital angular momentum coupling of light in the experiment by using the resonance of resonant ultrahigh-order modes (UOMs). A linear-polarized light is incident into the birefringent symmetrical metal cladding planar waveguide at the near-normal incident angle θ_i, and excites a high density of UOMs inside the waveguide [32–35]. The experiment shows a transverse spatial deviation at a submillimeter scale in the reflected light corresponding to two opposite spins, which can be visibly seen on the CCD. Our work points out a unique platform for studying the fundamental physics of the ultrastrong spin-orbital angular momentum coupling of light without applying the quantum weak measurement, leading towards broad potential implications including quantum information, optical communications, and biosensing.

We start with a brief description on the physical picture of the spin-orbital angular momentum coupling of light by considering a plane wave incident on a surface. Under the

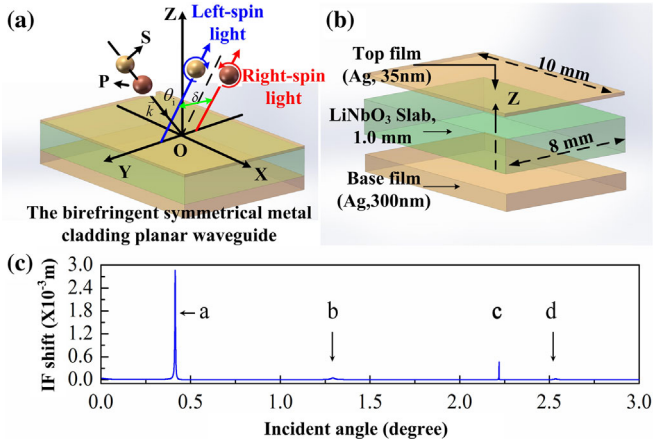

FIG. 1. Spin-orbital angular momentum coupling of light on the birefringent symmetrical metal cladding planar waveguide and the polarization-dependent resonances. (a) The physical picture of SHEL. (b) 3D schematic diagram of the birefringent symmetrical metal cladding planar waveguide. (c) IF shift is calculated by the transfer-matrix method. Peaks *a* and *c* are due to the *p*-polarized resonance, while peaks *b* and *d* are related to the *s*-polarized resonance [37].

transverse momentum conservation after the reflection, the polarizations associated with the plane-wave components experience different rotations due to the optical spin-orbit interaction. In the spin basis set, the polarization states correspond to $|H\rangle = (1/\sqrt{2})(|+\rangle + |-\rangle)$ and $|V\rangle = (-i/\sqrt{2})(|+\rangle - |-\rangle)$. Here, H (V) represents horizontal (vertical) polarization. $|+\rangle$ ($|-\rangle$) corresponds to left-(right-)circularly polarized light [LCPL (RCPL)]. In the lowest-order approximation, the change of one polarization state $|H\rangle$ after the reflection gives $|k_y\rangle|H\rangle \rightarrow |k_y\rangle(|H\rangle + k_y\delta|V\rangle) = |k_y\rangle|\varphi\rangle$ with $\phi = k_y\delta \ll 1$. In the spin basis, $|\varphi\rangle = (1/\sqrt{2})[\exp(-ik_y\delta)|+\rangle + \exp(ik_y\delta)|-\rangle]$, which can be written in the matrix form with $\exp(-ik_y\hat{\sigma}_3\delta)$ giving the interaction between the spin and the transverse momentum of light [36]. Expressions of the reflected angular spectrum can be written as [37]

$$|\phi_r^H\rangle = \frac{1}{\sqrt{2}}[\exp(ik_{ry}\delta^H_{r|+\rangle})|+\rangle + \exp(-ik_{ry}\delta^H_{r|-\rangle})|-\rangle], \quad (1)$$

$$|\phi_r^V\rangle = \frac{i}{\sqrt{2}}[-\exp(ik_{ry}\delta^V_{r|+\rangle})|+\rangle + \exp(-ik_{ry}\delta^V_{r|-\rangle})|-\rangle]. \quad (2)$$

Here, $\delta^H_{r|\pm\rangle} = \mp(1+r_s/r_p)\cot\theta_i/k_0$, $\delta^V_{r|\pm\rangle} = \mp(1+r_p/r_s)\times\cot\theta_i/k_0$, and $k_0 = 2\pi/\lambda_0$. λ_0 is the wavelength of incident light, θ_i is the incident angle, and r_s (r_p) is the Fresnel reflection coefficient for the s (p) polarization at θ_i [see Fig. 1(a)]. Hence, in Eqs. (1) and (2), the terms $\exp(\pm ik_{ry}\delta^H_{r|\pm\rangle})$ and $\exp(\pm ik_{ry}\delta^V_{r|\pm\rangle})$ indicate the spin-orbit coupling terms in the case of horizontal and vertical polarizations of photons.

We consider the incident Gaussian beam with the H polarization. From the boundary condition, we obtain relations $k_{rx} = -k_{ix}$ and $k_{ry} = k_{iy}$ for the incident (k_{iy}) and reflected (k_{ry}) optical momenta reciprocal to the Y axis. From Eqs. (1) and (2), we have the general expressions of the reflected field [37]

$$|\Psi_r^H\rangle = \frac{r_p}{\sqrt{2}}[\exp(ik_{ry}\delta^H_{r|+\rangle})|+\rangle + \exp(-ik_{ry}\delta^H_{r|-\rangle})|-\rangle], \quad (3)$$

$$|\Psi_r^V\rangle = i\frac{r_s}{\sqrt{2}}[-\exp(ik_{ry}\delta^V_{r|+\rangle})|+\rangle + \exp(-ik_{ry}\delta^V_{r|-\rangle})|-\rangle], \quad (4)$$

with

$$\delta^H_{r|\pm\rangle} = \mp\frac{\lambda}{2\pi}\left[1 + \frac{|r_s|}{|r_p|}\cos(\phi_s - \phi_p)\right]\cot\theta_i,$$
$$\delta^V_{r|\pm\rangle} = \mp\frac{\lambda}{2\pi}\left[1 + \frac{|r_p|}{|r_s|}\cos(\phi_p - \phi_s)\right]\cot\theta_i, \quad (5)$$

where $\varphi_{p,s}$ is the phase of the Fresnel reflection coefficient. The similar expressions have been applied several times in the literature [26,36,41–44].

In Eq. (5), $|\delta^{H,V}_{r|+\rangle} - \delta^{H,V}_{r|-\rangle}|$ gives the separation of the reflected RCPL and LCPL with the incident light at the polarization H or V, which corresponds to the splitting of opposite spin photons as the result of the spin-orbit interaction in light propagation. This quantity denotes the transverse shift (i.e., IF shift) [31]. The general strategy for enhancing such a shift is to achieve a large $|r_p|/|r_s|$ or $|r_s|/|r_p|$ [10–13]. For instance, one uses the polarization-dependent resonance such as SPR to reduce the reflectivity of one polarization to 10^{-4} in a practical experiment, and to achieve an enhancement factor up to 10^2. The resulting IF shift reaches to the micrometer scale and therefore one can observe it by using the quantum weak measurement technology [12–18].

On the other hand, with a large $|r_p|/|r_s|$ or $|r_s|/|r_p|$, the IF shift can be further enhanced by increasing $\cot\theta_i$ in Eq. (5). One notices that $\cot\theta_i$ approaches infinite as θ_i reduces to zero. Therefore, considering a case with the incident angle $\theta_i < 1$ degree and $|r_p|/|r_s| = 10$, one can find the estimated total enhancement factor is ~570. It therefore gives a submillimeter scaled IF shift in theory. Achieving such an enhancement by utilizing the term $\cot\theta_i$ in the experiment desires the polarization-dependent resonances at the near-zero incidence. Here, we show the possibility of achieving the increase of $\cot\theta_i$ together with a large $|r_p|/|r_s|$ or $|r_s|/|r_p|$ by using the UOMs in our designed waveguide, and hence realizing an IF shift at the order of submillimeter, which can be directly distinguishable by human eyes.

The UOMs are the oscillating standing modes bounded in millimeter thick metal-dielectric-metal structure as shown in Fig. 1(b), which is referred to as the symmetrical metal cladding planar waveguide [32–35]. In such a waveguide, the use of the thin metal coupling layer ($d \sim 30$ nm) and the small effective refractive index ($n_{\text{eff}} < 1$) enables the direct coupling of light from the free space into the guiding layer without any additional coupler such as grating or high-index prism [12,20–23]. Moreover, the relatively thick guiding layer sandwiched between two metal layers can support thousands of guided modes, which obey the dispersion relation

$$\kappa d = m\pi + 2\arctan\left|\rho\frac{\alpha}{\kappa}\right|, \qquad (m = 1, 2, 3, \ldots), \quad (6)$$

where $\rho = 1$ for TE(s) modes, while $\rho = \varepsilon_1/\varepsilon_2$ for TM(p) modes. m is an integer and denotes the mode order. The vertical propagation constant κ in the guiding layer and the decay coefficient α in the metal claddings are defined by $\kappa = (k_0^2\varepsilon_1 - \beta^2)^{1/2}$ and $\alpha = (\beta^2 - k_0^2\varepsilon_2)^{1/2}$, where k_0 is the wave number in the free space, ε_1 and ε_2 represent the dielectric constants of the dielectric and the metal films, respectively, and $\beta = k_0 N$ is the transverse propagation constant with the effective refractive index N for all guided modes. The expression for κ can be rewritten as $\kappa = k_0(\varepsilon_1 - N^2)^{1/2}$. One can find that β approaches zero when θ_i goes to zero. The second term on the right-hand side of Eq. (6) is usually ignored since it goes to nearly zero for the experimental condition $m > 10^3$. We therefore can expand Eq. (6) near $\theta_i = 0$, which reads

$$\cos\theta_{i,m} \approx m\frac{\lambda}{2\sqrt{\varepsilon_1}d}, \qquad (7)$$

where $\theta_{i,m}$ refers to the resonant incident angle for the mth UOM. From Eq. (7), we notice that there exists an UOM with an integer $m_0 \approx [2\sqrt{\varepsilon_1}d/\lambda]$, which makes $\cos\theta_{i,m_0} \sim 1$. Hence, in our designed optical structure, a near-zero ($\theta_{i,m_0} \sim 0$) incidence of light can be efficiently coupled into the resonant mode inside the guiding layers, which not only makes it possible to achieve a significant large $|\delta^{H,V}_{r|+\rangle} - \delta^{H,V}_{r|-\rangle}|$ associated to the SHEL, but also generates a sufficiently large signal. It should be noted that Eq. (7) is only valid for the small incident angle θ_i while one can find the more accurate way to calculate the reflectivity of the layered structure via the transfer-matrix method [37].

Here, we compare three structures with the SPR scheme, Brewster's angle, and UOMs, respectively [37], with similar parameters and calculate the possible incident angle of light at resonant couplings. We choose $|r_s|/|r_p| \sim 9$ for all three structures. For cases with the SPR scheme and Brewster's angle, one obtains θ_i as 43.72° and 56.30°,

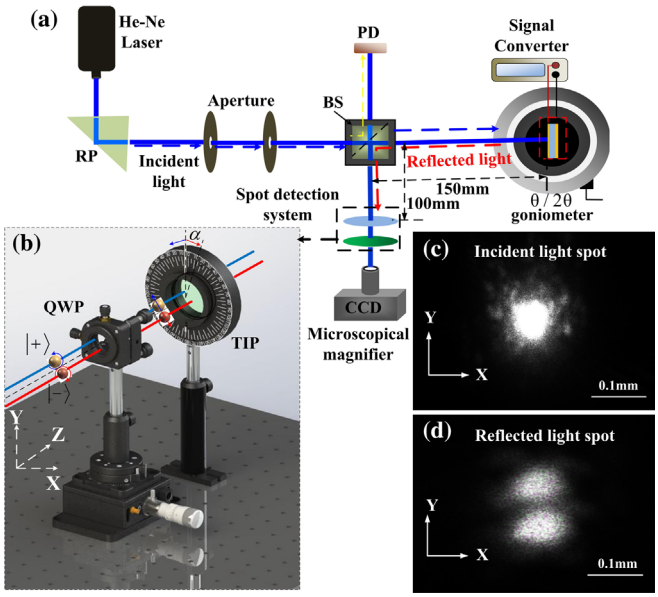

FIG. 2. Experimental setup and intensity distributions of incident and reflected light. (a) Experimental setup. (b) Spot detection system. (c) and (d) the CCD image and the intensity of incident light spot, respectively. The CCD image and the intensity distribution of reflected light spot, respectively. QWP: quarter-wave plate; TIP: tunable linear polarizer; BP: beam splitter.

respectively, which leads to the enhancement factor $\cot\theta_i < 0.9$ for both cases [36,41–44]. This gives $|\delta^{H,V}_{r|+\rangle} - \delta^{H,V}_{r|-\rangle}| < 0.9\lambda/2\pi$, corresponding to a nanometer order of magnitude that requires the quantum weak measurement for the observation in the experiment. As a comparison, for the birefringent symmetrical metal cladding planar waveguide with UOMs, we plot the simulation results of $|\delta^{H,V}_{r|+\rangle} - \delta^{H,V}_{r|-\rangle}|$ with the incident angle varying from 0° to 3.0° in Fig. 1(c). For a peak value of $|r_s|/|r_p|$, the corresponding coupling angle θ_i is ~0.47°, $|\delta^{H,V}_{r|+\rangle} - \delta^{H,V}_{r|-\rangle}| > 10^3\lambda/2\pi$, which exhibits a significant enhancement for SHEL [37]. It therefore makes it possible to reach the submicrometer IF shift for the direct measurement of SHEL in the experiment, which we demonstrate in the following.

The experimental setup is shown in Fig. 2(a). A pump laser beam from a 632.8 nm He-Ne laser (model TEM_{00}), with an incident power of 25 mW, knocks on a beam splitter. The reflected beam from the beam splitter is collected by a photodetector which is used to monitor the output power. The corresponding transmission beam passes the linear collimating system, and then illuminates on the surface of the birefringent symmetrical metal cladding planar waveguide hold on a rotation stage. The stage is controlled by a step motor linked to the computer which can be rotated precisely. By rotating the stage, the incident angle of light is tuned, so we can excite the desired UOMs of the waveguide at the coupling angle. The reflected light from the waveguide is projected onto a

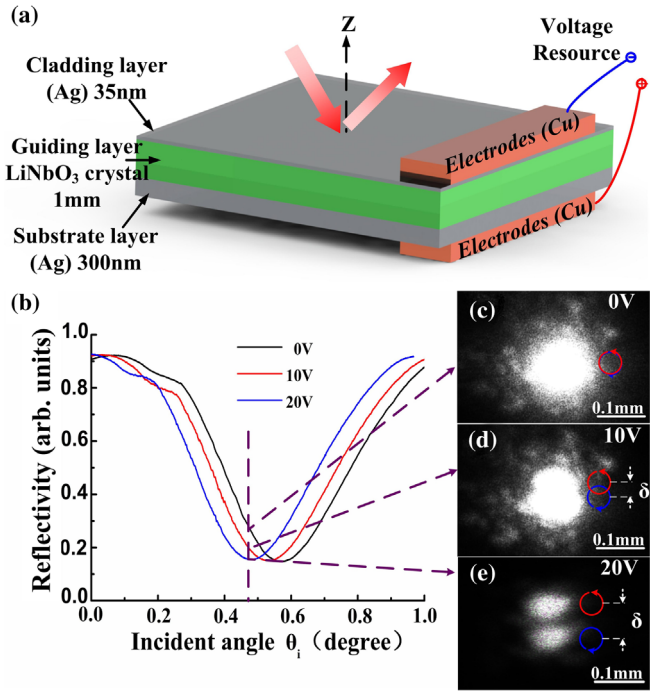

FIG. 3. The splitting in the reflected light spot for different external applied voltages. (a) 3D schematic diagram of the birefringent symmetrical metal cladding planar waveguide. (b) The measured reflection spectra for TM (p) polarization at different applied voltages. (c)–(e) The experimental measurement of polarization dependent splitting in the reflected light spot for external voltages as 0, 10, and 20 V, respectively. The incident angle is fixed at 0.47 degree [see the dashed line in (b)].

screen and captured by the CCD. A spot detection system, constructed by a quarter-wave plate and a linear polarizer [see Fig. 2(b)], can be used before the light gets into the CCD. With this additional spot detection system, one can distinguish the polarization nature of light, i.e., spin $|+\rangle$ and spin $|-\rangle$ components in the collected signal, by changing the angle α between the mean axis of the linear polarizer and vertical axis.

We first show the images and intensity distributions of the incident light as well as the reflected light from the waveguide in CCD, respectively, in Figs. 2(c) and 2(d). One can directly see that the reflected light exhibits two separated spots for the incident angle being $\theta_i = 0.57°$ in the experiment. Meanwhile, compared to the spot of the incident light, the brightness of each spot of the reflected light has been reduced, and the corresponding area of illumination expands towards both directions along the Y axis.

To present the resonance of the incident light coupling into the waveguide by exciting the UOMs, we show the experimental results of the collected reflected light with different incident angles in Fig. 3. Figure 3(b) displays plots of the reflectivity vs the incident angle with three different external voltages, which are voltage applied on two surfaces of waveguide layers to change the effective refractive index. As indicated in Eq. (6), the resonance of the corresponding UOM is modified by the voltage. Therefore, one finds that three plots of the reflectivity in Fig. 3(b) exhibit the dip (i.e., the resonance) at different coupling angles. In particular, a specific resonant dip for TM (p) polarization locates at $\theta_i = 0.57°$ without the external voltage, and θ_i is shifted to 0.47° when the applied voltage is 20 V. We fix $\theta_i = 0.47°$, and plot the intensity distributions of the reflected light under different external voltages in Figs. 3(c)–3(e). The separation of spots is clearly observed once the resonance of the corresponding UOM is excited. The maximum value of the separation is ~0.16 mm. For a nonresonant excitation as shown in Fig. 3(c), we detect a single large spot in the experiment.

To determine the spin nature of the separated spots in both Figs. 2 and 3, we measure the degree of polarization (DOP) in the experiment. The spot detection system including a quarter-wave plate and a linear polarizer splits the right- and left-circularly polarization of light. The fast axis of the quarter-wave plate is placed at a 45° to the X axis, while the axis of the polarizer or the angle α can be tuned [see Fig. 2(b)]. Therefore, the DOP of the reflected light can be calculated by the formalism $|(I_{\max} - I_{\min})/(I_{\max} + I_{\min})|$ [37], where $I_{\max}$ ($I_{\min}$) refers to the maximal (minimal) integral value of the intensity over the cross section for each spot while changing α. The experimental results of the intensity integral over the X axis with a range of α from 0° to 90° as well as Y are plotted in Fig. 4(a), where one can see that the intensity of one spot near $Y = 150$ μm is decreasing with the increase of α while the intensity of the other spot near $Y = 260$ μm is increasing. The intensities of two spots are changing at a period of 180°. We plot the intensity distribution of the reflected light for cases with the axis of the polarizer chosen as vertically and horizontally, respectively, in Figs. 4(b) and 4(c). We find that the spot near $Y = 260$ μm has the maximum integral value $V = 128.65$ in Fig. 4(b), and it has the minimum value $V = 5.06$ in Fig. 4(c). Similar phenomena can be found for the other spot. From experimental results, we calculate the DOPs for the right- and left-circularly polarized spots, which gives ~0.924 and ~0.832, respectively. This measurement indicates that two spots exhibit the opposite spin nature. The accuracy of this measurement shall be enhanced if a higher-quality polarizer is used.

In the experiment, we show that the reflected light exhibits two separated spots when the resonance of UOM is excited by the incident light. Each spot corresponds to the spin nature of light. A ~0.16-mm separation between two spots (or two spins) in Fig. 3(e) has been measured, indicating a significant IF shift due to the ultrastrong spin-orbital angular momentum coupling of light. The excitation of UOM is extremely important here to support a strong optical spin-orbital coupling. If there is no UOM resonance as shown in Fig. 3(c), the incident light

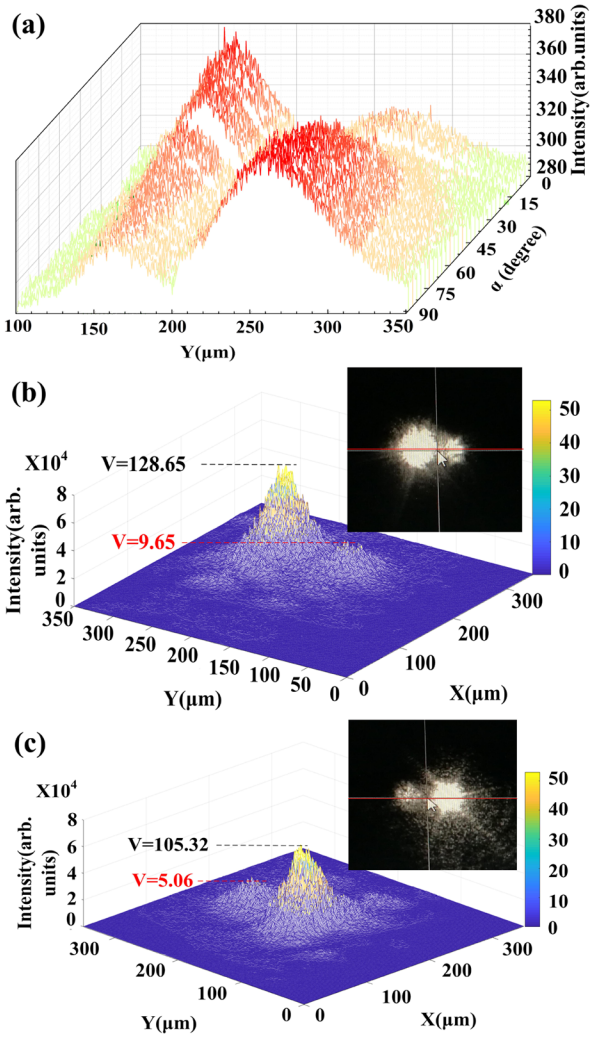

FIG. 4. The Y intensity distributions of the reflected light with the spot detection system as the axis of polarizer α in the spot detection system rotates from 0° to 90°. (a) The change of the intensity integral over the X axis. (b) and (c) the images of the two orthogonally polarized light spots as the polarizer is placed with $\varphi = 90°$ and $\varphi = 0°$, respectively, of the value of V is calculated by integrating the intensity over the cross section of each of the spots.

gets directly reflected from the surface of the waveguide, and hence there is no separation between two spins of light.

In conclusion, we demonstrate an enhanced spin-orbital angular momentum coupling of light with an IF shift ~0.16 mm in experiment, where the UOMs inside the birefringent symmetrical metal cladding planar waveguide is excited for the near-normal incident light at the visible-wavelength regime. Such a transverse shift is visible to human eyes. Our work hence points out a unique route for efficiently manipulating the polarization degree of freedom of light to harvest various functionalities in a broad range of photonic technologies including filters, sensors, and beam splitters, as well as the quantum metrology.

This work was supported by the National Key R&D Program of China (Grants No. 2018YFA0306301, No. 2017YFA0303701) and the National Natural Science Foundation of China (NSFC) (No. 11734011, No. 11764020, No. 11974245); and the Foundation for Development of Science and Technology of Shanghai (No. 17JC1400400).

The authors declare that they have no conflict of interest.

*yuanluqi@sjtu.edu.cn
†xfchen@sjtu.edu.cn

[1] X. H. Ling, X. X. Zhou, K. Huang, Y. C. Liu, C. W. Qiu, H. L. Luo, and S. C. Wen, Rep. Prog. Phys. **80**, 066401 (2017).
[2] K. Y. Bliokh and A. Aiello, J. Optics **15**, 014001 (2013).
[3] K. Y. Bliokh, F. J. Rodriguez-Fortuno, F. Nori, and A. V. Zayats, Nat. Photonics **9**, 796 (2015).
[4] C. Imbert, Phys. Rev. D **5**, 787 (1972).
[5] F. I. K. Fedorov, Dokl. Akad. Nauk SSSR **105**, 465 (1955).
[6] G. Jayaswal, G. Mistura, and M. Merano, Opt. Lett. **39**, 2266 (2014).
[7] F. Töppel, M. Ornigotti, and A. Aiello, New J. Phys. **15**, 113059 (2013).
[8] M. R. Dennis and J. B. Götte, New J. Phys. **14**, 073013 (2012).
[9] M. Onoda, S. Murakami, and N. Nagaosa, Phys. Rev. Lett. **93**, 083901 (2004).
[10] A. Aiello, P. Banzer, M. Neugebauer, and G. Leuchs, Nat. Photonics **9**, 789 (2015).
[11] O. Takayama, J. Sukham, R. Malureanu, A. V. Lavrinenko, and G. Puentes, Opt. Lett. **43**, 4602 (2018).
[12] G. A. Wurtz, R. Pollard, W. Hendren, G. P. Wiederrecht, D. J. Gosztola, V. A. Podolskiy, and A. V. Zayats, Nat. Nanotechnol. **6**, 107 (2011).
[13] F. J. Rodríguez-Fortuño, G. Marino, P. Ginzburg, D. O'Connor, A. Martínez, G. A. Wurtz, and A. V. Zayats, Science **340**, 328 (2013).
[14] Q. He, S. Sun, and L. Zhou, Research **2019**, 1849272 (2019).
[15] C. F. Li, Phys. Rev. A **76**, 013811 (2007).
[16] K. Y. Bliokh, I. V. Shadrivov, and Y. S. Kivshar, Opt. Lett. **34**, 389 (2009).
[17] X. H. Ling, X. X. Zhou, W. X. Shu, H. L. Luo, and S. C. Wen, Sci. Rep. **4**, 5557 (2015).
[18] S. Murakami, N. Nagaosa, and S. C. Zhang, Science **301**, 1348 (2003).
[19] S. Goswami, M. Pal, A. Nandi, P. K. Panigrahi, and N. Ghosh, Opt. Lett. **39**, 6229 (2014).
[20] N. Hermosa, A. M. Nugrowati, A. Aiello, and J. P. Woerdman, Opt. Lett. **36**, 3200 (2011).
[21] L. Cai, M. X. Liu, S. Z. Chen, Y. C. Liu, W. X. Shu, H. L. Luo, and S. C. Wen, Phys. Rev. A **95**, 013809 (2017).
[22] X. Yin, Z. Ye, J. Rho, Y. Wang, and X. Zhang, Science **339**, 1405 (2013).
[23] A. Shaltout, J. J. Liu, A. Kildishev, and V. Shalaev, Optica **2**, 860 (2015).
[24] A. Farmani, M. Miri, and M. H. Sheikhi, J. Opt. Soc. Am. B **34**, 1097 (2017).
[25] Q. D. Jiang, H. Jiang, H. Liu, Q. F. Sun, and X. C. Xie, Phys. Rev. Lett. **115**, 156602 (2015).

[26] J. M. Menard, A. E. Mattacchione, H. M. van Driel, C. Hautmann, and M. Betz, Phys. Rev. B **82**, 045303 (2010).
[27] F. Pillon, H. Gilles, S. Girard, M. Laroche, R. Kaiser, and A. Gazibegovic, J. Opt. Soc. Am. B **22**, 1290 (2005).
[28] X. J. Tan and X. S. Zhu, Opt. Lett. **41**, 2478 (2016).
[29] X. Jiang, Q. Wang, J. Guo, J. Zhang, S. Chen, X. Dai, and Y. Xiang, J. Phys. D **51**, 145104 (2018).
[30] H. L. Luo, X. X. Zhou, W. X. Shu, S. C. Wen, and D. Y. Fan, Phys. Rev. A **84**, 043806 (2011).
[31] M. Kim, D. Lee, T. H. Kim, Y. Yang, H. J. Park, and J. Rho, ACS Photonics **6**, 2530 (2019).
[32] H. Lu, Z. Cao, H. Li, Q. Shen, and X. Deng, Opt. Lett. **31**, 386 (2006).
[33] Y. Wang, H. Li, Z. Cao, T. Yu, Q. Shen, and Y. He, Appl. Phys. Lett. **92**, 061117 (2008).
[34] Y. Wang, Z. Cao, T. Yu, H. Li, and Q. Shen, Opt. Lett. **33**, 1276 (2008).
[35] H. Li, Z. Cao, H. Lu, and Q. Shen, Appl. Phys. Lett. **83**, 2757 (2003).
[36] H. Luo, X. H. Ling, X. X. Zhou, W. X. Shu, S. C. Wen, and D. Y. Fan, Phys. Rev. A **84**, 033801 (2011).
[37] See Supplemental Material at http://link.aps.org/supplemental/10.1103/PhysRevLett.124.053902, which includes the reflected angular spectrum of the layered structure, the thin film transfer matrix, the numerically calculated and estimated IF shifts, the piezoelectric effect of waveguide structure, and the degree of polarization (DOP), which includes Refs. [7,8,32,34,35,38–40].
[38] F. Chen, Z. Cao, Q. Shen, and Y. Feng, Appl. Opt. **44**, 5393 (2005).
[39] X. Liu, Z. Cao, P. Zhu, Q. Shen, and X. Liu, Phys. Rev. E **73**, 056617 (2006).
[40] C. Yin and Z. Cao, Phys. Rev. A **80**, 064102 (2009).
[41] Y. Qin, Y. Li, F. Xiao, Z. Liu, H. He, Y. Xiao, and Q. Gong, Opt. Express **18**, 16832 (2010).
[42] A. Aiello, M. Merano, and J. P. Woerdman, Phys. Rev. A **80**, 061801(R) (2009).
[43] X. Zhou, Z. Xiao, H. Luo, and S. Wen, Phys. Rev. A **85**, 043809 (2012).
[44] A. Kavokin, G. Malpuech, and M. Glazov, Phys. Rev. Lett. **95**, 136601 (2005).